Supplementary Information (SI) for Soft Matter.

Mesoscale Polymer Arrays: High Aspect Ratio Surface Structures and Their Digital Reconstruction

Demi E. Moed[a], Michael S. Dimitriyev[b], Benjamin R. Greenvall[a], Gregory M. Grason[a,]*, Alfred J. Crosby[a,]*

a. Department of Polymer Science and Engineering, University of Massachusetts Amherst, Amherst, MA 01003, USA
b. Department of Materials Science and Engineering, Texas A&M University, TX 77840, USA

Corresponding authors:
* crosby@mail.pse.umass.edu, grason@mail.pse.umass.edu

Computationally-Quantified Morphology: A Detailed Overview

Image Processing. The microscopy data is deconvolved using NIS-Elements' automatic algorithm and exported to Fiji for processing. We blur the Z-stacks using a 3D gaussian filter then binarize the images via thresholding at value *t*, skeletonize the 3D dataset using Fiji's built-in algorithm, and export the result to a .tiff stack.[1] We manually adjust the binarization threshold *t* for stack of images sample to balance the visibility of the dimmest ribbons with the oversaturation of bright, proximal segments (Fig 3a-c).

Coding Overview. We use a proprietary MATLAB algorithm to evaluate the morphology of our ribbon arrays. The objective of the code is to first determine the position of individual ribbons in 3D space from the confocal data, and then use the estimated ribbon positions to extract key metrics from the data, such as the radius of curvature, the inter-ribbon separation, and the distribution of mass density relative to the substrate surface. Due to the wide variety of ribbon architectures exhibited across experiments, this strategy allows for a quantitative approach to compare visually distinct morphologies. This code uses strategies from [2–7] to guide its design.

Skeletonization and Segmentation. The code takes in the skeletonized .tiff stack and locates the individual (x,y,z) coordinates of each skeleton voxel (Figure S3a), with each voxel having dimensions of 1 px x 1 px x 1 z-step. Each voxel is classified as an end point, a junction, or a backbone based on the number of pixels in its neighborhood[2] and neighboring backbones are connected to create segments terminated at either end points or junctions (Figure S3b)[2,3].

Bridging Junctions. The algorithm groups proximal junctions and then identifies the segments that connect to each. To bridge the junctions, we must first describe the direction of each segment's approach. However, because the ribbons can follow relatively tortuous paths, we must first subdivide each ribbon segment into smaller components. In this way, we isolate the region of each segment closest to the junction.

To do this, we define the tortuosity of a ribbon as the difference in the distance between the ribbon's end-to-end distance and its total length. Starting at one end, we trace the segment point-by-point, and once the tortuosity exceeds an empirically-defined threshold, we terminate the growing subsegment and begin a new one.[2] In this way, segments with low curvature are broken into fewer regions of more voxels, and high curvature segments are described by a greater number of subsegments, each containing fewer voxels.

This process leaves us with a list of skeleton subsegments, each described as an n x 3 matrix, with each row containing the x, y, and z, coordinates of a voxel. We consider each of these voxels to have equal

mass. Using the *cov* function, we compute the gyration tensor of each individual subsegment. The largest principal eigendirection of that gyration tensor is the directionality of the subsegment (Figure S3c).

We calculate the principal eigendirection of each subsegment immediately bordering the junction and determine all possible dot products between them (Figure S3d). We draw the initial pathways between segments that are the most parallel and should therefore exhibit the largest dot product. The algorithm makes these connections while searching for and ignoring spurious segments– artifacts of the skeletonization process[2,6] – based on the following criteria:

(a) The segment approaches an odd-numbered intersection at an angle perpendicular to all other segments
(b) The segment shares significant (>80%) overlap with another segment in x and y, with a slight (<10 z-step) z-offset.
(c) The segment exhibits improbable straightness, with tortuosity $\left(\frac{L_{path}}{L_{e-e}}\right)$ approaching 1.

Buildup and Evaluation. Once the initial connections (Figure 3e) are made, the algorithm then begins building up connections between segments can be made based on two criteria:

(a) The end points of two segments are within a maximum distance (5 voxels) of one another. In the event that multiple end points meet this criterion, the connection is made to between the segments whose approach is most parallel.
(b) The segments' ends exhibit direct overlap.

The quality of the resulting guess is then evaluated, making the following assumptions about each ribbon:

(a) A ribbon can only have two end points, and therefore cannot branch.
(b) A ribbon is continuous, and therefore cannot have any gaps along its backbone.
(c) A ribbon follows a unique path, and therefore should not have significant overlap with other segments.
(d) Each ribbon is tethered to a substrate at only one end.

If a ribbon fails to pass these criteria, it is broken up based on the criteria that it failed and re-evaluated as separate segments. Ribbons that share >90% of their points with another segment are combined into a single segment. Furthermore, if >20% of a ribbon's points intersect with others, the entire tangle is re-evaluated to determine the most probable path for each ribbon. In this instance, all possible combinations of paths between end points are evaluated to minimize:

(a) The number of points excluded from the buildup
(b) The average number of overlapping points between each of the pathways
(c) The average tortuosity of each proposed pathway
(d) The average difference in path lengths

Buildup and evaluation steps are iterated to generate a final estimate (Figure 3g). All segments containing less than 30 points are excluded from consideration. The remaining ribbons are smoothed using MATLAB's *rloess* method due to the method's tolerance of outliers in the data. The window used to smooth these curves is proportional to the size of the segment, and then all (x,y,z) coordinates are translated into micron-based positions based on the micron-to-pixel ratio and the size of the z-step. Z-values are corrected to align the lowest z-values with a height of zero.

The algorithm then identifies and removes the portions of ribbons located along the laser cutting line. These ribbons are adhered to the substrate and therefore will not exhibit morphological changes as the

environment changes. The algorithm considers all ribbons that are within 20 μm from the slide and less than 200 μm in length, and then it identifies the average location of these ribbons along the *y*-axis. The laser cutting line to which the ribbons are tethered runs perpendicular to the *y*-axis, and therefore the ribbon fragments located along the center line should exhibit a similar range in *y*-values. The algorithm considers the most frequent range in *y*-values to be the location of the center axis. The code then removes all points within 20 μm of the substrate that fall within this *y*-range. This removes the substrate-bound portion of the ribbon from future consideration.

Quantitative Metrics. We quantify the ribbon position using the following metrics:

(a) **Curvature**: determined using the first and second derivatives of the ribbon's coordinates. Assuming the (x,y,z) coordinates of a ribbon trace a path $F(t)$, with a step size of $dt = 1$, then the curvature κ can be approximated:

$$\text{(Eq. S1)}\ \kappa = \frac{\left||F'(t)\times F''(t)|\right|}{||F'(t)||^2}$$

(b) **Radius of curvature**: the inverse of the curvature.

(c) **Straightness**: All radius of curvature values greater than the targeted length of the ribbon (1000 μm) are ignored, and the ribbon is considered to be perfectly straight in these regions. The total number of straight points along the ribbon backbone normalized by the number of points along the ribbon length is calculated as a measured of ribbon straightness.

(d) **Lateral mass distribution**: The center axis of the laser cutting line is defined by the central line of the excluded region along the laser cut. The average y distance between each ribbon and between the entire set of ribbons relative to this central axis is calculated.

(e) **Vertical mass distribution**: each point along the ribbon skeleton is considered to carry the same weight. To determine the height of each ribbon's center-of-mass, the z-coordinates of each ribbon's points are averaged. To determine the vertical distribution of the entire slide, the average of all z-coordinates is evaluated independent of ribbon of origin.

(f) **End-to-end distance**: the Euclidian distance between each ribbon's end points.

(g) **Inter-ribbon separation**: All ribbons other than the ribbon of interest are converted into a point cloud. The distance between each point along the ribbon of interest and its nearest neighbor in the point cloud is determined. The code then averages these distances across each individual ribbon, as well as recorded independently of their associated ribbon

(h) **Number of inter-interactions**: As the width of the ribbons can be up to 20 μm, we consider ribbons are close enough to interact with one another if they are within 10 μm of each other. We identify and count the number of instances where the inter-ribbon separation is less than or equal to this cutoff.

(i) **Length**: Sum of the distance between each pair of neighboring points along the ribbon backbone.

Derivation of Curvature and Relaxation Time Equations

The total energy U of a ribbon, as a function of time t, is given by:

$$\text{(Eq. S2)}\ U(t) = \int_0^L \mathrm{d}s \left\{\frac{1}{2} E I_{yy} \kappa^2(s,t) - \left(\gamma P \Delta X_y\right)\kappa(s,t)\right\}$$

Where *E* is the Young's modulus, I_{yy} is the second moment of area of the ribbon's cross-section, $\kappa(s,t)$ is the curvature at position s and time t, P is the cross-sectional perimeter, and ΔX_y is the offset between

the centers of the ribbon's cross-sectional perimeter and cross-sectional area. Assuming that the ribbon lies along the *x*-axis with its thickness along the *y*-axis, its moment about the *z*-axis, $M_z(s,t)$ is described as

$$\text{(Eq. S3) } M_z(s,t) = EI_{yy}\kappa(s,t) - \gamma P \Delta X_y$$

We assume that the ribbon deforms only in the *xy*-plane, and is therefore described by the reduced Kirchhoff rod equilibrium equations, namely[8]

$$\text{(Eq. S4) } \frac{d\boldsymbol{F}}{ds} = -\boldsymbol{f}(s,t), \text{ and}$$

$$\text{(Eq. S5) } \frac{dM_z}{ds} = (\boldsymbol{F}(\mathrm{s,t}) \times \hat{\boldsymbol{t}}(s,t))_z \, .$$

Here, $\hat{\boldsymbol{t}}(s,t)$ is the unit tangent vector along the ribbon, and $\boldsymbol{F}(\mathrm{s,t})$ is the internal force along the ribbon and $\boldsymbol{f}(s,t)$ is the external force density along the ribbon.

We next assume that each segment of the ribbon is subject to Stokes drag. Therefore, each point $\boldsymbol{r}(s,t)$ along the ribbon will experience a force proportional to the velocity $\boldsymbol{v}(s,t) = \partial_t \boldsymbol{r}(s,t)$. The force per unit length is given by

$$\text{(Eq. S6) } \boldsymbol{f}(s,t) = -\zeta \frac{d\boldsymbol{v}}{ds} \, ,$$

where ζ is a drag coefficient. By integrating over *s*, the internal force becomes

$$\text{(Eq. S7) } \boldsymbol{F}(\mathrm{s,t}) - \boldsymbol{F}(0,t) = \zeta \int_0^s ds' \frac{d\boldsymbol{v}}{ds'} = \zeta\big(\boldsymbol{v}(s,t) - \boldsymbol{v}(0,t)\big) \, .$$

Finally, we assume that the ribbon is attached to the substrate at $s = 0$, leading to the boundary conditions $\boldsymbol{v}(0,t) = 0$ and $\boldsymbol{F}(s,t) = 0$, and thus

$$\text{(Eq. S8) } \boldsymbol{F}(\mathrm{s,t}) = \zeta \boldsymbol{v}(s,t) \, .$$

When considering the moment balance, we express the velocity at segment *s* in terms of the local tangent and normal frame $\hat{\boldsymbol{n}}$ as

$$\text{(Eq. S9) } \boldsymbol{v}(s,t) = v_t(s,t)\hat{\boldsymbol{t}}(s,t) + v_n(s,t)\hat{\boldsymbol{n}}(s,t)$$

Noting that the tangential component v_t does not contribute to the moment M_z and $\hat{\boldsymbol{t}} \times \hat{\boldsymbol{n}} = \hat{\boldsymbol{z}}$, we simplify the mechanical equilibrium condition to

$$\text{(Eq. S10) } \frac{dM_z}{ds} = -\zeta v_n(s,t) \, .$$

We next assume that the ribbon is constrained to lie flat against the substrate for $s \leq 0$, which corresponds to the position of the ribbon anchor. The ribbon curves along the interval $0 < \mathrm{s} < \mathrm{L}$, so integrating Eq. S10 from $s = 0$ to $s = \mathrm{L}$, we find that

$$\text{(Eq. S11) } M_z(L,t) = -\zeta \int_0^L \mathrm{d}s v_n(s,t) = -\zeta L \langle v_n \rangle(t) \, ,$$

where the normal component of the velocity averaged along the length of the ribbon is represented as

$$\text{(Eq. S12) } \langle v_n \rangle(t) = \frac{1}{L}\int_0^L \mathrm{d}s v_n(s,t) \, .$$

We consider a minimal model of ribbon shape that satisfies the shape constraints, namely

$$\text{(Eq. S13) } \boldsymbol{r}(x,t) = \hat{\boldsymbol{x}}x + \hat{\boldsymbol{y}}\frac{k(t)}{2}x^2 \text{ ,}$$

where positions along the ribbon are expressed in terms of the x-coordinate. To leading order in the small deflection approximation, $s \approx x$ and furthermore

$$\text{(Eq. S14) } \hat{\boldsymbol{t}}(x,t) = \frac{\mathrm{d}\boldsymbol{r}}{\mathrm{d}s} \approx \hat{\boldsymbol{x}} + \hat{\boldsymbol{y}}k(t)x \text{ ,}$$

$$\text{(Eq. S15) } \hat{\boldsymbol{n}}(x,t) = \hat{\boldsymbol{z}} \times \hat{\boldsymbol{t}}(x,t) \approx \hat{\boldsymbol{y}} - \hat{\boldsymbol{x}}k(t)x \text{ , and}$$

$$\text{(Eq. S16) } \kappa(x,t) = \frac{\mathrm{d}^2\boldsymbol{r}}{\mathrm{d}s^2} \cdot \hat{\boldsymbol{n}}(x,t) \approx k(t) \text{ .}$$

The normal component of the velocity and its average are therefore

$$\text{(Eq. S17) } v_n(x,t) = \frac{1}{2}\dot{k}x^2 \text{ and}$$

$$\text{(Eq. S18) } \langle v_n \rangle(t) \approx \frac{1}{L}\int_L^0 \mathrm{d}x v_n(x,t) \approx \frac{1}{6}\dot{k}L^2 \text{ .}$$

This yields the moment balance:

$$\text{(Eq. S19) } \dot{k} + \frac{6EI_{yy}}{\zeta L^2}k(t) = \frac{6\gamma P \Delta X_y}{\zeta L^2} \text{ .}$$

We integrate and assume that $k(0) = 0$ to yield

$$\text{(Eq. S20) } k(t) = \kappa_o\left(1 - e^{-\frac{t}{\tau_o}}\right) \text{ ,}$$

where

$$\text{(Eq. S21) } \kappa_o = \frac{\gamma P \Delta X_y}{EI_{yy}} \text{ and}$$

$$\text{(Eq. S22) } \tau_o = \zeta L^2/6EI_{yy}$$

Given that $I_{yy} \sim wh^3$ and that the drag coefficient of long, thin rods can be approximated as[9]

$$\text{(Eq. S23) } \zeta \approx \frac{4\pi\eta L}{\ln\left(\frac{L}{w}\right)}$$

we can therefore solve for the relaxation time:

$$\text{(Eq. S24) } \tau_o \sim \frac{\eta}{E}\frac{L^3}{wh^3 \ln\left(\frac{L}{w}\right)} \text{ .}$$

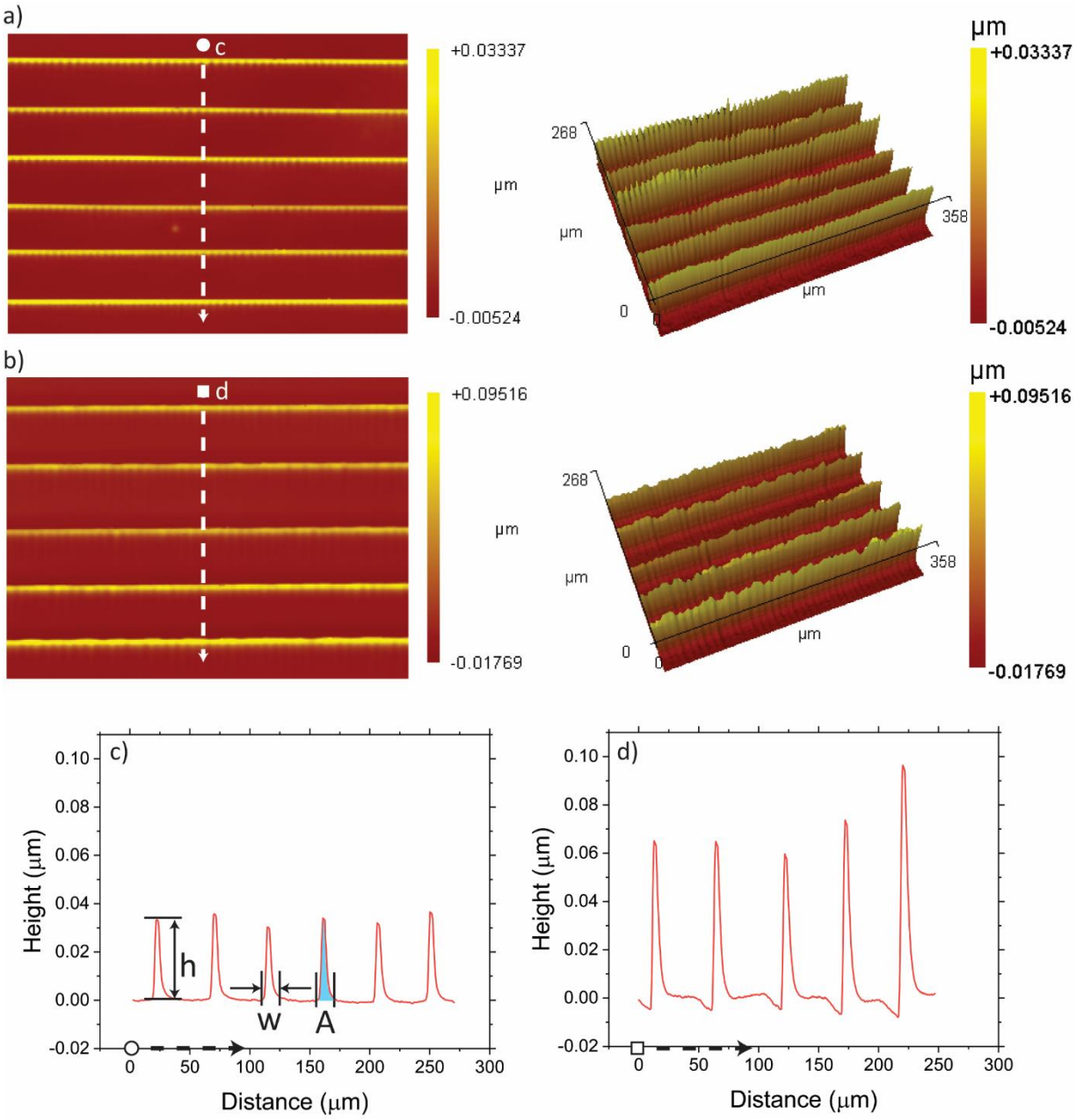

Figure S1. Optical profilometry profiles of two different samples, measured to have an average thickness of (a) 36 nm + 7nm and (b) 73 nm + 40 nm across the slide, respectively. The dashed lines along the thickness profiles correspond to the x-axes of (c) and (d), which plot thickness as a function of location along said axis. Here, each peak corresponds to an individual ribbon of thickness *h*, width *w*, and cross-sectional area *A*.

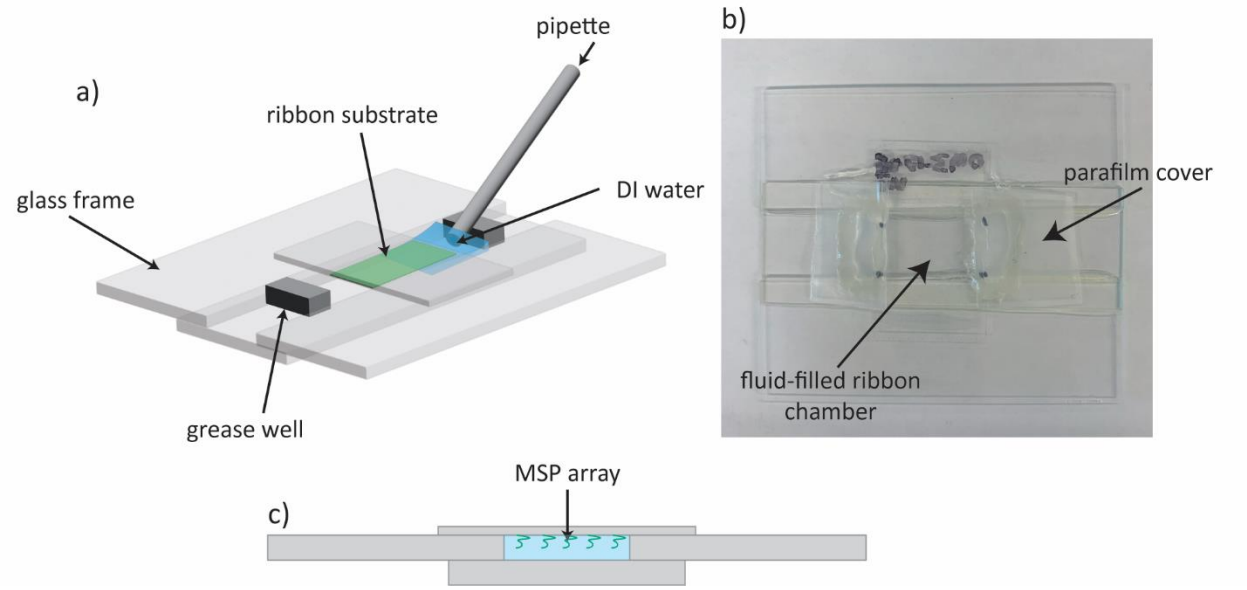

Figure S2. Model of a unidirectional flow chamber used for confocal microscopy. (a) A 3D-model of the flow chamber with essential parts labelled. (b) A top-down view of a sample flow chamber sealed with parafilm. (c) A side-view of the flow chamber, with the ribbon array hanging from the cover slip that forms the ceiling of the flow chamber. The ribbons remain fully-submerged in water for the duration of the experiment.

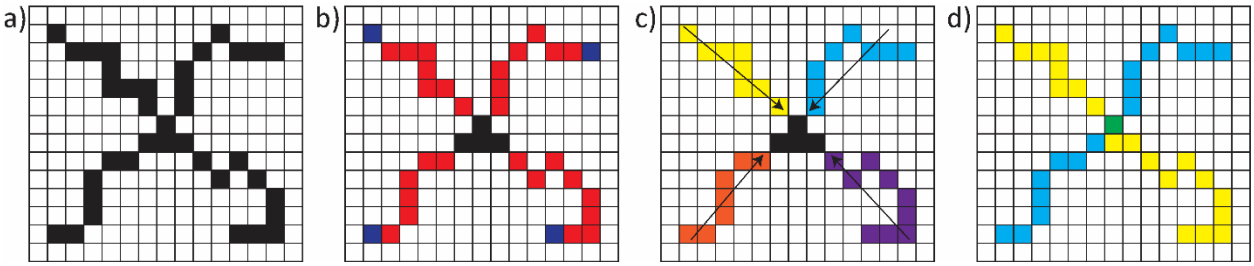

Figure S3. A 2D representation of the process of building up ribbons in 3D. (a) Individual (x,y) pixel values are sorted (b) into end points (blue), backbones (red), and junctions (black). (c) Neighboring pixels and backbones are connected, and their directionality relative to their neighboring junction is identified. (d) The final buildup of two ribbons (yellow, blue) and their overlapping sections (green).

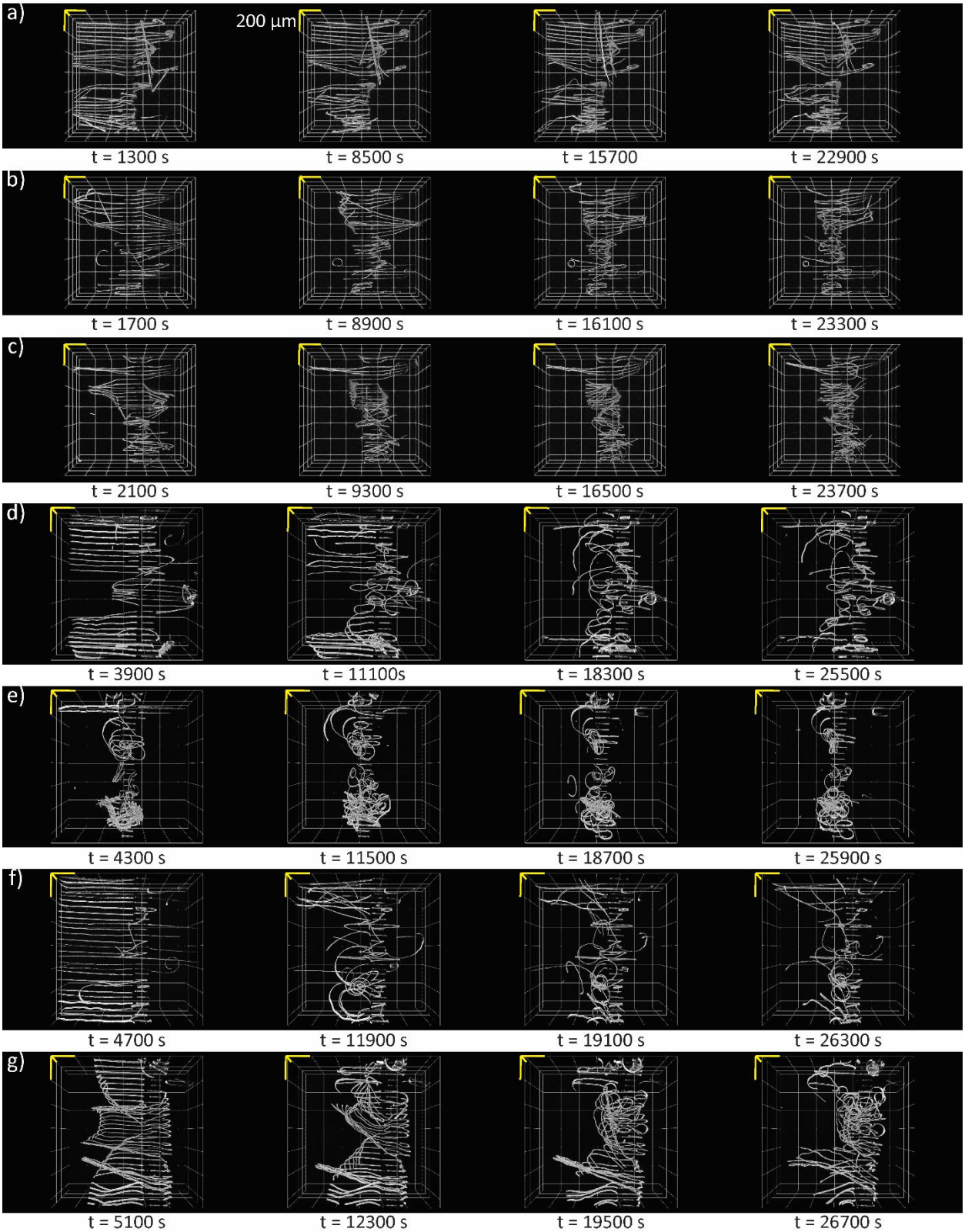

Figure S4. Morphological changes of (a-c) 72 nm and (d-g) 36 nm thick MSP ribbon arrays. All scale bars represent 200 µm.

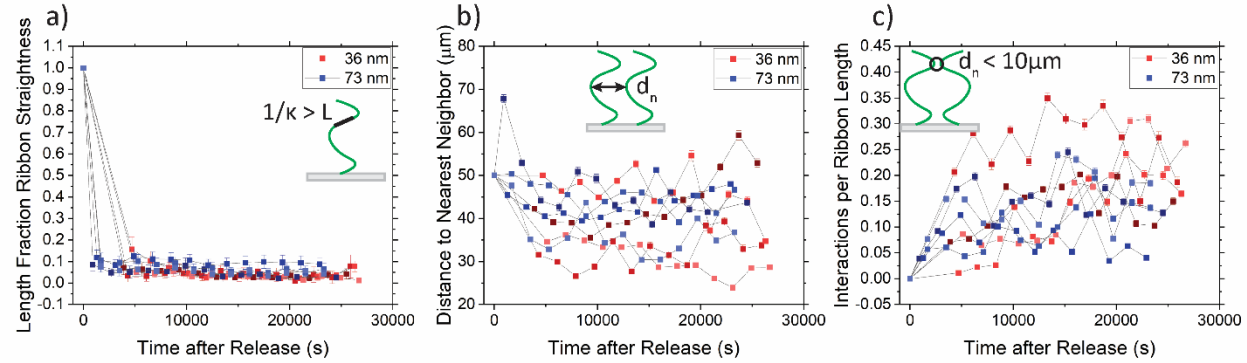

Figure S5. Additional computationally-determined quantitative descriptors. (a) The fraction of each ribbon length wherein the radius of curvature (1/κ) is greater than the theoretical ribbon length, suggesting that the ribbon is perfectly straight in these regions. (b) The average nearest neighbor distance between ribbons. (c) The fraction of instances where the distance between nearest neighbor ribbons are less than the width of a ribbon, suggesting that the surfaces are close enough to interact. All error bars correspond to a 95% confidence interval.

References

1 X. Feng, C. J. Burke, M. Zhuo, H. Guo, K. Yang, A. Reddy, I. Prasad, R. M. Ho, A. Avgeropoulos, G. M. Grason and E. L. Thomas, *Nature*, 2019, **575**, 175–179.

2 X. Huang, D. Wen, Y. Zhao, Q. Wang, W. Zhou and D. Deng, *Results Phys*, 2016, **6**, 170–177.

3 G. Gaiselmann, I. Manke, W. Lehnert and V. Schmidt, *Image Analysis and Stereology*, 2013, **32**, 57–63.

4 L. R. Gómez, N. A. García and T. Pöschel, *Proc Natl Acad Sci U S A*, 2020, **117**, 3382–3387.

5 P. Latil, L. Orgéas, C. Geindreau, P. J. J. Dumont and S. Rolland du Roscoat, *Compos Sci Technol*, 2011, **71**, 480–488.

6 J. Lux, *Image Analysis and Stereology*, 2013, **32**, 13–25.

7 G. Gaiselmann, R. Thiedmann, I. Manke, W. Lehnert and V. Schmidt, *Comput Mater Sci*, 2012, **59**, 75–86.

8 B. Audoly and Y. Pomeau, *Elasticity and Geometry: From Hair Curls to the Non-linear Response of Shells*, OUP Oxford, 2010.

9 M. Doi and S. F. Edwards, *The Theory of Polymer Dynamics*, Clarendon Press, 1988.